RSC Advances

ROYAL SOCIETY OF CHEMISTRY

www.rsc.org/advances

Preparation of Ag-MnO_2/graphene composite for the oxygen reduction reaction in alkaline solution

Shengwei Liu, Xue Qin*

Department of Chemistry, School of Science, Tianjin University, and Collaborative Innovation Center of Chemical Science and Engineering（Tianjin), Tianjin 300072, China

Corresponding Author Tel.: +86 022 27403670 E-mail address: qinxue@tju.edu.cn

ABSTRACT

Ag-MnO_2/graphene composite with mesoporous structure is prepared by immersion-calcination method. The composite composed of Ag (~6 nm) and MnO_2 (~4 nm) nanoparticles are distributed evenly on the graphene sheets. The oxygen reduction peak of the Ag-MnO_2/graphene catalyst in a 0.1 M KOH solution is tested at −0.15 V, which is more positive than that of 20% Pt/C (−0.19 V). The onset potential of Ag-MnO_2/graphene (0.068 V) is close to Pt/C (0.079 V). The oxygen reduction reaction limiting current density for the Ag-MnO_2/graphene catalyst is approximately 5.62 $mAcm^{-2}$, which is similar to that for Pt/C (5.83 $mAcm^{-2}$). The onset potential of the Ag-MnO_2/graphene is close to the Pt/C. The introduction of Ag nanoparticles between the MnO_2 nanoparticles on graphene sheets can significantly improve the catalytic activation, because of the increase in conductivity and abundant active sites provided during ORR process.

1. Introduction

The oxygen reduction reaction (ORR), which is the main cathodic reaction for some clean energy technologies, has great significance for metal air batteries and fuel cells [1,2]. Currently, the widely used catalysts for ORR in acidic media are Pt and Pt

alloys because of their stability. However, the high cost of Pt materials is one of the obstacles for the commercialization of fuel cells. Meanwhile, some non-Pt electrocatalysts, such as carbon-supported metals and transition metal oxides (Pd/C, Ag-MnOx/C), have been investigated extensively to catalyze the ORR in alkaline environments. In addition, the kinetics of the ORR in alkaline solution is superior to that in acidic media [3–6].

Among the nanomaterials, silver is highly active toward the ORR in alkaline solution. This condition is because of high electrical conductivities, antibacterial properties, and excellent catalytic properties [7]. However, Ag nanoparticles are likely to aggregate because of the extremely high surface energy. Thus, Ag nanoparticles are usually supported on conductive supports, such as like graphene and carbon, to enhance the surface area of the active sites [8]. However, the activity of silver toward the ORR is not satisfactory and must be improved.

In recent years, MnO_2 has been widely investigated as one of the most promising candidates for the ORR in alkaline solution, because this substance is naturally abundance and low cost, and it has high energy density and environmental compatibility [9–12]. However, the active phases of the MnO_2 reported in the literature are still in conflict, and the catalytic performance of MnO_2 nanostructures toward the ORR is highly dependent upon the crystalline phases of the chemical composition. For example, the orders was β-MnO_2 < λ-MnO_2 < γ-MnO_2 < α-MnO_2 ≈ δ-MnO_2 for different crystal forms of MnO_2 [13]. The advantages of silver and manganese oxides have been combined by preparing an Ag-MnO_2/C catalyst [14,15].

In this study, a facile method was developed to prepare Ag-MnO_2/graphene composite. The as-prepared graphene was obtained with the use of an exfoliated

graphite oxide through thermal annealing, which is the support of the Ag-MnO_2 catalyst for ORR in alkaline solution. The composite has excellent electrocatalytic performance, because Ag nanoparticles significantly increase in conductivity, surface area and active sites, which are favorable for ORR.

2. Experiment

2.1. Preparation of catalyst.

Analytical grade $AgNO_3$ and 50wt.% $Mn(NO)_3 \cdot 4H_2O$ were used without further purification. Pt/C (20wt.%) was purchased from Johnson Mattey.

The Ag-MnO_2/graphene composite was synthesized through a simple method: First, Graphite oxide (GO) was prepared from natural graphite with a modified Hummers method [16]. The GO powders was reduced through thermal annealing at 400 ℃ for 60 min in N_2 flow to achieve graphene [17]. 0.025 g $Mn(NO)_3$ was added into the homogeneous suspension of 0.05 g graphene in 20 mL absolute ethyl alcohol and ultrasonicated for 15 min, followed by adding 0.01 g $AgNO_3$ and ultrasonicated for 15 min. The solvent was then evaporated under an infrared lamp, and the composite powder was subjected to thermal decomposition at 320 ℃ for 45 min in a N_2 atmosphere. The sample was then cooled down to room temperature, and the Ag-MnO_2/graphene composite was successfully obtained. MnO_2/graphene and Ag/graphene composites were synthesized through the same process of the above without addition of $AgNO_3$ and $Mn(NO)_3$, respectively.

2.2. Physical characterization.

The Ag-MnO_2/graphene composite and MnO_2/graphene were characterized through X-ray diffraction (XRD, D/MAX-2500), Raman spectroscopy (In Via Rflex),

Transmission electron microscopy (TEM, Tecnai G2 F20), scanning electron microscopy (SEM, S4800) equipped with an energy dispersive X-ray analyzer (EDX), and X-ray photoelectron spectroscopy (XPS, PHI1600).

2.3. Preparation of modified electrodes and electrochemical measurements.

All half-cell experiments for the ORR were conducted under the same conditions where Ni-mesh and Hg/HgO were used as counter and reference electrodes, respectively. Catalyst paste was prepared by ultrasonically mixing 6.0 mg of the as-prepared sample with a certain amount of 5 wt.% Nafion solution for 30 min to create a homogeneous suspension. The prepared catalytic paste was transferred to the surface of a glassy carbon electrode with a diameters o f 3 mm. Finally, the ink was dried under an infrared lamp to form a thin catalyst film on a glass carbon electrode as a working electrode.

The cyclic voltammograms (CVs) were obtained at different scan rates with a rotation rate of 1200 rpm in a 0.1 M KOH solution, saturated with N_2 and O_2, correspondingly. The linear sweep voltammograms (LSVs) were obtained under the process of saturated with O_2 in a 0.1 M KOH solution at different rotation rates with scan rate of 1 mV/s, A rotating disk electrode (RDE, ATA-1B, China) and an electrochemical workstation (CHI604C, ShangHai Chen Hua, China) were used for to obtain CVs and LSVs.

3. Results and discussion

3.1. Physical characterization of the composite.

The Ag-MnO_2/graphene composite as well as graphene, MnO_2/graphene and Ag/graphene were characterized using Raman spectroscopy. As presented in Figure 1,

all of the spectra display two prominent peaks at 1355 and 1587 cm^{-1}, which can be assigned to the D and G bands, respectively. After thermal annealing treatment, the Raman D/G intensity ratios of the Ag-MnO_2/graphene and MnO_2/graphene composites (where the D peak is a defect peak caused by interval scattering [18], and G refers to the graphene G peak) are lower than that of the as-made graphene, because the thermal reduction actually increased the average size of the crystalline graphene domains in the as-prepared Ag-MnO_2/graphene and MnO_2/graphene composite [19]. Meanwhile, the bands located at 480 and 640 cm^{-1} in the spectra of the Ag-MnO_2/graphene and MnO_2/graphene composites are contributed to the symmetric stretching vibrations of Mn-O of MnO_2 [20], which confirms the presence of the MnO_2 in the as-prepared composite. The peak at the 640 cm^{-1} in the composite of Ag-MnO_2/graphene increases dramatically compared with MnO_2/graphene and Ag/graphene. This result can be attributed to the surface enhanced Raman scattering from the intense local electromagnetic fields of Ag nanoparticles that accompany Plasmon resonance [21], which demonstrates the effective combination of Ag and MnO_2 nanoparticles on graphene sheets.

Figure 2 displays the XRD patterns of graphene, MnO_2/graphene, Ag/graphene and Ag-MnO_2/graphene. For all of the composites, the broadened peaks located at approximately 24.5 ° are assigned to graphite (002) of the graphene support. Meanwhile, the peaks located at approximately 18.12 °, 28.84 °, 37.52 °, and 60.27 ° for the MnO_2/graphene, correspond to the (200), (310), (211), and (521) crystalline planes. The main diffraction peaks match well with the standard peaks of α-MnO_2 (JCPDS 44-0141). Meanwhile, the XRD results of Ag-MnO_2/graphene composite show four new diffraction peaks located at about 38.1 °, 44.3 °, 65.4 °, and 77.3 °, which can be indexed to the (111), (200), (220), and (311) reflections of the face-centered

cubic phase Ag (JCPDS No. 65-2871), the four peaks corresponding well to the peaks of Ag/graphene composite. The results further indicate the successful preparation of Ag and MnO_2 nanoparticles on graphene sheets.

TEM images of the as-synthesized Ag-MnO_2/graphene composite are shown in Figure 3. The nanoparticles cover the surface of graphene sheets with a uniform distribution (Figures 3a–3b). The images show that the nanoparticles with different contrasts can be observed on the graphene sheets. 7.5 wt.% of nanoparticles with darker contrasts can be attributed to the Ag particles because silver is a heavy atom and has a strong scattering factor for electrons [22], whereas the nanoparticles with lighter contrasts can be denoted as MnO_2. The high magnification image (the inset in Figure 3b) shows that the sizes of Ag and MnO_2 nanoparticles are about 6 and 4 nm, respectively. The lattice fringes in the image with a high magnification provide further evidence for distinguishing MnO_2 and Ag nanoparticles. The lattice distance of 0.24 nm that was detected in the darker contrast particles can be assigned to the (111) plane of phase Ag, and the lattice distance of 0.20 nm can be indexed to the (310) plane of MnO_2. The TEM images show that the structural distribution of the nanoparticles offers abundant active sites in electrochemical reactions.

The content of Ag and MnO_2 can be calculated using EDX to be 7.5 wt.% and 32.5 wt.%, respectively. The selected overall area of SEM (Figure 3c) for mapping, as shown in Figures 3d–3f, showed presence of Ag-MnO_2/graphene through distinctive elements, such as C, Mn, and Ag. The elemental mapping of Mn and Ag shows that the amount of silver element has significantly less manganese, which confirms the homogeneous distribution of Ag and MnO_2 nanoparticles. This results is consistent with the TEM results.

The special surface area is 426.4 m^2g^{-1} (Figure 4) for Ag-MnO_2/graphene, which is larger than that of simplex nano-MnO_2 (35.2 m^2g^{-1}) [23]. The introduction of Ag nanoparticles and graphene significantly increases the surface area from 35.2 to 426.4 m^2g^{-1}. The pore-size distribution (the inset in Figure 4) is centered at 2–3 nm, which demonstrates that the mesoporous nature of the Ag-MnO_2/graphenecomposite. The structures provide more chances for oxygen atoms to contact catalyst and enhance the electrolyte contact area, thereby advancing the ORR.

XPS was used to probe the chemical states of Mn and Ag in the Ag-MnO_2/graphene composite. The XPS spectrum of Ag-MnO_2/graphene composite (Figure 5) further confirms the presence of Ag and Mn elements. Figure 5a shows the XPS spectrum of the Mn 2p signal of Ag-MnO_2/graphene. The Mn 2p XPS spectrum exhibits two major peaks with binding energy values at 653.5 and 642.4 eV, which can be attributed to the Mn $2p_{1/2}$ and Mn $2p_{2/3}$. Whereas the Mn $2p_{2/3}$ peak can be deconvoluted into two peaks at 642.2 and 641.1 eV, which are ascribed to the Mn(IV) and Mn (III) species [24]. Figure 5b presents the typical Ag 3d spectrum of Ag-MnO_2/graphene composite, the peaks of Ag $3d_{3/2}$ and $3d_{5/2}$ can be observed at 374.2 eV and 368.2 eV, respectively, which demonstrates that Ag is present in the metallic state [25,26]. The XPS results agree with that from the Raman and XRD analyses.

3.2. Electrochemical characteristics of the composites.

The CVs for the Ag-MnO_2/graphene composite at 1200 rpm of the rotation rate in a 0.1 M KOH solution has a scanning rate of 5 mV/s with N_2-saturated and O_2-saturated, respectively. As shown in Figure 6a, two existing peaks of the electrode with an Ag-MnO_2/graphene catalyst in O_2-saturated solution for negative scanning are located at approximately 0.16 V and –0.15 V, respectively. However, only a peak of the

electrode with Ag-MnO_2/graphene catalyst located approximately 0.16 V in N_2-saturated electrolytes. This result indicates that the oxygen reduction peak of the electrode with Ag-MnO_2/graphene catalyst is observed at –0.15 V. The inset of Figure 6a shows that a cathodic peak in O_2-saturated electrolyte of the electrode with Pt/C located at approximately –0.19 V is compared with the peak in N_2-saturated electrolyte, which demonstrates that the electrochemical activation of Ag-MnO_2/graphene catalyst to catalyze ORR is more positive than that of Pt/C (–0.19 V). Meanwhile, the current density of the oxygen reduction peak of Ag-MnO_2/graphene catalyst is larger than that of the Pt/C catalyst. The increase in the current density and peak potential for the electrode with Ag-MnO_2/graphene catalyst indicates high catalytic of Ag-MnO_2/graphene toward ORR. An obscure peak at approximately –0.05 V can be attributed to the formation of MnOOH from MnO_2 [27], which is masked by the oxygen reduction peak at –0.15 V. Figure 6b shows the CV of Ag-MnO_2/graphene electrode at different scan rates of 2 mV/s to 20 mV/s. The cathodic peak currents are linear to the square root of the scan rate, as shown the inset in Figure 6b. These facts indicate a diffusion control for the ORR process, and confirm that the immobilized Ag-MnO_2/graphene is stable.

The CV curves of MnO_2/graphene and Ag/graphene composites are studied in a 0.1 M KOH solution with N_2-saturated and O_2-saturated, respectively, to investigated the interaction of silver and manganese dioxide on the catalytic activity of Ag-MnO_2/graphene composite and the catalytic mechanism of oxygen reduction, as shown in Figure 7a–7b. For the CV curve of MnO_2/graphene (Figure 7a), a pronounced peak at approximately –0.29 V in O_2-saturated solution is contributed to the oxygen reduction of the electrode with MnO_2/graphene composite. Meanwhile, the reduction peak at approximately –0.17 V in N_2-saturated and O_2-saturated

solutions is assigned to the IV valence of MnO_2, which is reduced to MnOOH. According to the CV curve of Ag/graphene composite shown in Figure 7b, the cathodic peak at approximately 0.16 V of the electrode with Ag/graphene composite exists both in O_2-saturated and in N_2-saturated electrolytes, which is assigned to the transformation of silver oxides to metallic silver [4]. In addition, this condition can also explain the peak at approximately 0.16 V of the electrode with an Ag-MnO_2/graphene composite (Figure 6a). The reduction peak at approximately –0.35 V of the electrode with Ag/graphene in O_2-saturated is attributed to the oxygen reduction. The catalytic activity of the Ag-MnO_2/graphene catalyst is more positive than that of Ag/graphene and MnO_2/graphene composites. Moreover, the current density of Ag-MnO_2/graphene is larger than that of Ag/graphene and MnO_2/graphene composites because of the synergy of silver and manganese dioxide,.

According to the above analysis, the catalytic property of Ag-MnO_2/graphene can be attributed to the synergy between silver and manganese dioxide nanoparticles, and the introduction of Ag nanoparticles, which increases the surface area of MnO_2/graphene. The MnO_2/graphene catalyzes the ORR mechanism of the peak at approximately –0.17 V, which could cause reduction of O_2 to HO_2^- as described in Eq.(1). Thus, the peak at approximately –0.29 V shows the electrochemical transition of HO_2^- to OH^- (Eq.(2)) [28,29].

$$O_2(g) + H_2O(l) + 2e^- \rightarrow HO_2^-(l) + OH^-(l) \quad (1)$$

$$HO_2^-(l) + H_2O(l) + 2e^- \rightarrow 3OH^-(l) \quad (2)$$

The reaction of Eq. (1) can be explained using the mechanism of reaction because manganese dioxide adsorbed the oxygen as shown in the following equation [30]:

$$MnOOH(s) + O_2(g) \rightleftharpoons MnOOH\cdots O_2(s) \quad (3)$$

$$MnO_2(s) + H_2O(l) + e^- \rightleftharpoons MnOOH(s) + OH^-(l) \quad (4)$$

$$MnOOH\cdots O_2(s) + e^- \rightleftharpoons MnO_2(s) + HO_2^-(l) \quad (5)$$

Therefore, the reactions in Eq. (3)–(5) is equal to the Eq. (1), which corresponds to the common konwledge that O_2 reduction occurs simultaneously with MnO_2 reduction.

Therefore, the oxygen reduction peak of the electrode with an Ag-MnO_2/graphene catalyst is because the insertion of a proton into MnO_2 as the Eqs. (3) to (4), the Eq. (5) no longer appears in this process, which then produces synergistic effect with Ag, and the MnOOH adsorption of O_2 transfer to the surface of Ag, which can be explained using the mechanism of reaction, as shown in the following equations:

$$MnOOH\cdots O_2(s) + Ag(s) \rightleftharpoons MnOOH(s) + Ag\cdots O_2(s) \quad (6)$$

$$2Ag\cdots O_2(s\text{-}g) + H_2O(l) + 2e^- \rightarrow Ag_2O(s) + 2HO_2^-(l) \quad (7)$$

Ag may further facilitate the electrochemical reduction of HO_2^- as Eq. (2), thus the total reaction mechanism of the electrode with Ag-MnO_2/graphene at –0.05 V is:

$$2Ag(s) + 2MnO_2(s) + 3H_2O(l) + 2O_2(g) + 4e^- \rightarrow Ag_2O(s) + 2MnOOH(s) + 2OH^- + 2HO_2^-(l) \quad (8)$$

The instability of Ag_2O and MnOOH, allows these elements easily decompose into Ag and MnO_2, which continue catalyze the ORR circularly. Thus, the catalyst of Ag-MnO_2/graphene catalyzes O_2 to OH^- at –0.15 V. This result can be attributed to Eq. (8), which is equal to the combination of Eq. (1) and Eq. (2).

The LSV of the Ag-MnO_2/graphene composite was investigated between –0.7 V and 0.1 Vat a scan rate of 1 mV/s in O_2-saturated 0.1 M KOH solution with a rotation rate of 2400 rpm, as shown in Figure 8a. The ORR limiting current density for the Ag-MnO_2/graphene catalyst is approximately 5.62 $mAcm^{-2}$, which is larger than that of the Ag/graphene composite (0.92 $mAcm^{-2}$), and MnO_2/graphene composite (2.82 $mAcm^{-2}$), but similar to that of the Pt/C (5.83 $mAcm^{-2}$). The results indicate that Ag effectively improves electrical conductivity. Another critical factor determining the performance of a catalyst is the onset potential. The onset potential of Ag-MnO_2/graphene was detected at 0.068 V, which is close to that of Pt/C (0.079 V). The Tafel slope of Ag-MnO_2/graphene and Pt/C catalyst is 86 and 74 mV per decade, respectively, as shown in Figure 8b. The low ORR Tafel slope of Ag-MnO_2/graphene implies a transition from the Langmuirian absorption to the Temkin adsorption of adsorbed O/OH groups [31]. Therefore, the electrochemical catalyst activation of Ag-MnO_2/graphene composite is close to that of Pt/C for ORR.

The LSV of Ag-MnO_2/graphene at different rotation rates from 400–2400 rpm are shown in Figure 8c. The RDE data which were obtained through the Koutecky-Lecich equation are as follows [31,32].

$$\frac{1}{i} = \frac{1}{i_k} + \frac{1}{i_d}$$

$$i_k = nFkC_O$$

$$i_d = 0.62nFD_0^{2/3}\nu^{-1/6}C_0\omega^{1/2}$$

Where i_k and i_d represent the kinetics and diffusion limiting current densities (Am^{-2}), respectively. n is the electron number involved in ORR; F is the Faraday constant (96485 C mol^{-1}); k is the rate constant for ORR (m s^{-1}); D_0 is the diffusion coefficient of O_2 in solution (1.86×10^{-5} cm^2 s^{-1} in 0.1 M KOH); C_0 is the saturation

concentration of O_2 in solution (1.2 mM m^{-3} in 0.1 M KOH); v is the kinematic viscosity (0.0100810^{-6} cm^2 s^{-1} in 0.1 M KOH); and ω is the angular frequency of the rotation (rad s^{-1}). The electron transfer number (n) during ORR was calculated to be 3.5, 3.7, and 3.9 at –0.4 V, –0.5 V, and –0.6 V, respectively. The reaction mechanism of the near-four electron transfer pathway for the Ag-MnO_2/graphene catalyst further proves Eq. (8) [29,30]. The incorporation of Ag in α-MnO_2 improves the process of ORR efficiently.

In Figure 9, the impedance spectra of the MnO_2/graphene, Ag/graphene and Ag-MnO_2/graphene electrodes are consisted of one semicircle and a slope. Inset shows the equivalent circuit of the three electrodes, where R_0, R_1, R_2, CPE1, CPE2 and CPE3 are denoted as solution resistance, adsorption resistance, electrochemical reaction resistance, adsorption capacitance, double layer capacitance and diffusion capacitance, respectively. Because of the porous morphology of electrodes, a constant phase element (CPE) replaces the capacitor element reasonably. A CPE is usually defined as $\{Y (jw)\}^{-1}$. A nonlinear, least-square fitting calculation is performed using the equivalent circuit. For Ag/graphene electrode, the R_2 and CPE2 value (T) are 0.618 Ω g and 1.812 F g^{-1}, MnO_2/graphene electrode are 0.201 Ω g and 2.061 F g^{-1}, and Ag-MnO_2/graphene electrode 0.107 Ω g and 4.784 F g^{-1}. The R_2 of the MnO_2/graphene electrode is lower than that of the MnO_2/graphene and Ag/graphene electrodes. This further confirms that the electrical conductivity of Ag-MnO_2/graphene composite is improved significantly by the introduction of Ag nanoparticles, and the results consistent well with the polarization curves and CVs. The value of CPE2 is related to the true reaction areas of the electrode, so the double layer capacitance of Ag-MnO_2/graphene electrode is larger than that of the

MnO_2/graphene and Ag/graphene electrodes, which means Ag-MnO_2/graphene electrode has larger reaction area.

4. Conclusion

The Ag-MnO_2/graphene composite with a mesoporous structure was successfully prepared using immersion-calcination method. The Ag and MnO_2 nanoparticles are uniformly distribution on the graphene sheets. The CV curves show that the oxygen reduction potential of the Ag-MnO_2/graphene catalyst shifts positively by 200 and 140 mV compared with that of Ag/graphene and MnO_2/graphene composites, respectively, and even shift positively (40 mV) compared with that of 20% Pt/C. The activity of the Ag-MnO_2/graphene composite improved compared with that of 20% Pt/C. The results imply that the Ag-MnO_2/graphene composite is a promising catalyst for fuel cells in alkaline solution.

Acknowledgments

The authors gratefully acknowledge the financial support from the Open Project of Key Lab Adv. Energy Mat. Chem. (Nankai Univ.) (KLAEMC-OP201201) partially.

Reference

[1] Cheng, F. Y. Chem. Soc. Rev. 2012, **41**, 2172-2192.

[2] Neburchilov, V.; Wang, H.; Martin, J. J.; Qu, W. J. Power Sources 2010, **195**, 1271-1291.

[3] Chen, R.; Li, H.; Chu, D.; Wang, G. J. Phys. Chem. C 2009, **113**, 20689-20697.

[4] Guo, J.; Hsu, A.; Chu, D.; Chen, R. J. Phys. Chem. C 2010, **114**, 4324-4330.

[5] Ananth, M.V.; Giridhar, V.V.; Renuga, K. Int. J. Hydrogen Energy 2009, **34**, 658-664.

[6] Burchardt, T.; Gouérec, P.; Sanchez-Cortezon, E.; Karichev, Z.; Miners, J.H. Fuel 2002, **81**, 2151-2155.

[7] Sun, Y. G.; Xia, Y. N. Science 2002, **298**, 2176−2179.

[8] Yuan, L. Z.; Jiang, L.H.; Liu, J.; Xia, Z. X.; Wang, S. L.; Sun, G. Q. Electrochim. Acta 2014, **135**, 168-174.

[9] Cheng, F.; Su, Y.; Liang, J.; Tao, Z.; Chen, J. Chem. Mater. 2009, **22**, 898- 905.

[10] Zou, R.; Zhang, Z.; Yu, L.; Tian, Q.; Chen, Z.; Hu, J. Chem.–Eur. J. 2011, **17**, 13912–13917.

[11] Zhu, J.; He, J. ACS Appl. Mater. Interfaces 2012, **4**, 1770–1776.

[12] Cheng, F. Y.; Zhang, T. r.; Du, J.; Han, X. P.; Chen, C. C.; Chen, J.; Angew. Chem. Int. Ed. 2013, **52**, 2474-2477.

[13] Cao, Y. L.; Yang, H. X.; Ai, X. P.; Xiao, L. F. J. Electroanal. Chem. 2003, **557**, 127-134.

[14] Kostowskyj, M. A.; Kirk, D. W.; Thorpe, S. J. Int. J. Hydrogen Energy 2010, **35**, 5666-5672.

[15] Hu, F. P.; Zhang, X. G.; Xiao, F.; Zhang, J. L. Carbon 2005, **43**, 2931-2936.

[16] Wang, D. H.; Kou, R.; Choi, D. W.; Ynag, Z. G.; Nie, Z. M.; Li, J.; Saraf, L.V.; Hu, D. H.; Zhang, J. Graff, G. L. Liu, J;. Pope, M. A.; Aksay, I. A. ACS Nano 2010 , **4**, 1587-1595.

[17] Zangmeister, C. D. Chem. Mater. 2010, **22**, 5625-5629.

[18] Ferrari, A. C. Solid State Commun. 2007, **143**, 47-57.

[19] Wang, H. L.; Robinson, J. T.; Li, X. L.; Dai, H. J. J. Am. Chem. Soc. 2009, **131**, 9910-9911.

[20] Gao, T.; Glerup, M.; Krumeich, F.; Nesper, R.; Fjellvag, H.; Norby, P. J. Phys. Chem. C 2008, **112**, 13134–13140.

[21] Pasricha, R.; Gupta, A.; Srivastava, A. K. Small 2009, **5**, 2253–2259.

[22] Akita, T.; Kohyama, M.; Haruta, M. Acc. Chem. Res. 2013, **46**, 1773–1782.

[23] Wang, S. Y.; Xie, J. N.; Zhang, T. R.; Varadan, V. K. J. Power Sources 2009, **186** 523-538.

[24] Reddy, A. S.; Gopinath, C. S.; Chilukuri, S. J. Catal. 2006, **243**, 278–291.

[25] Zhou, Y. Z.; Yang, J.; He, T. T.; Shi, H. F.; Chen, X. N.; Lu, Y. X. Small 2013, **9**, 3445–3454.

[26] Ferraria, A. M.; Boufi, S.; Battaglini, N.; Rego, A. M. B.; Reivilar, M. Langmuir 2010, **26**, 1996–2001.

[27] Lima, F. H. B.; Calegaro, M. L.; Ticianeli, E. A. Electrochim. Acta 2007, **52**, 3732-3738.

[28] Verma, A.; Jha, A. K.; Basu, S. J. Power Sources 2005, **141**, 30-34.

[29] Cheng, F. Y.; Su, Y.; Liang, J.; Tao, Z. L. Chem. Mater. 2010, **22**, 898-905.

[30] Gao, H. L.; Li, Z. Y.; Xue, Q. J. Power Source 2014, **248**, 565-569.

[31] Goha, F. W. T.; Liu, Z. L.; Ge, X. M.; Zong, Y.; Du, G. J.; Hora, T. S. A. Electrochim. Acta 2013, **114**, 598–604.

[32] Hu, F. P.; Zhang, X. G.; Xiao, F.; Zhang, J. L. Carbon 2005, **43**, 2931-2936.

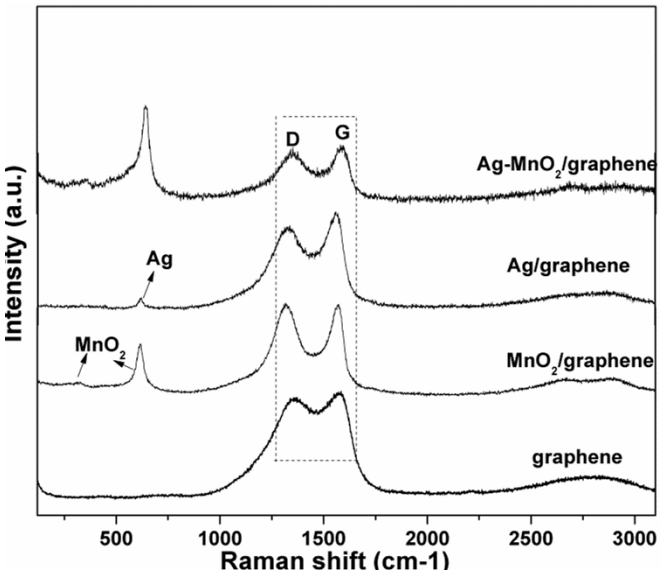

Figure 1. Raman spectra of graphene, MnO_2/graphene, Ag/graphene and Ag-MnO_2/graphene composites.

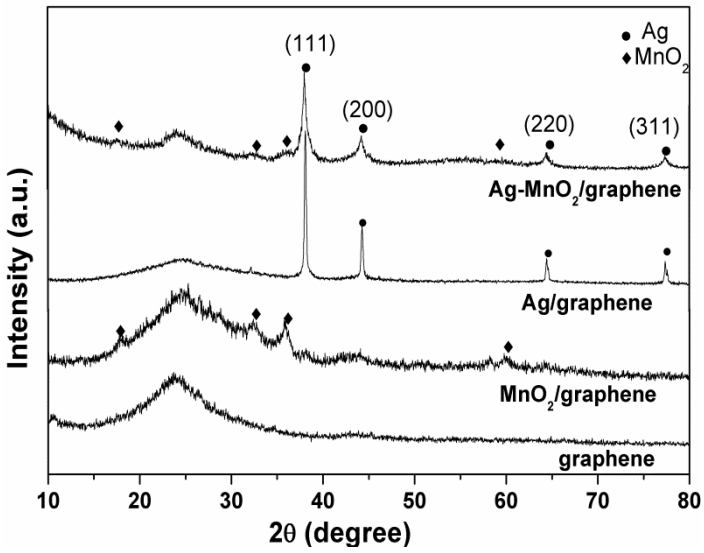

Figure 2. XRD patterns of graphene, MnO_2/graphene, Ag/graphene and Ag-MnO_2/graphene composites.

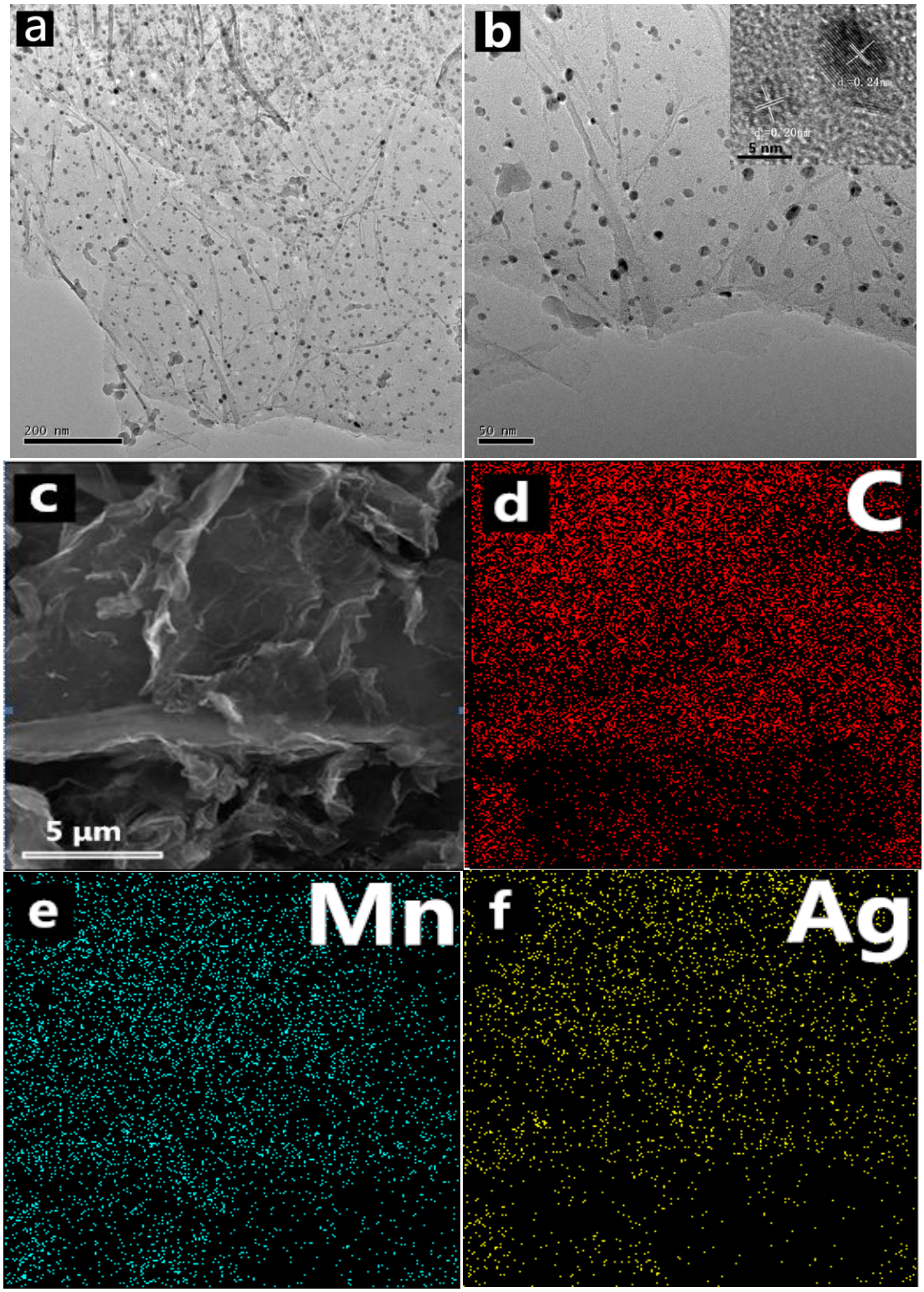

Figure 3. TEM images (a and b) of Ag-MnO_2/graphene composite and HRTEM (the inset of b) image of Ag and MnO_2 nanoparticles. (c) SEM images of Ag-MnO_2/graphene composite and (d, e, f) the EDX elemental mapping images of Ag-MnO_2/graphene composite.

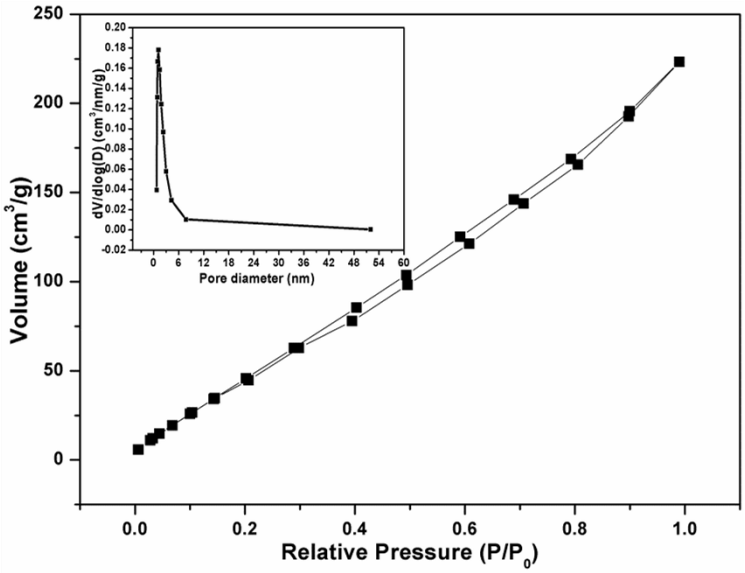

Figure 4. A typical N_2 adsorption isotherm of the Ag-MnO_2/graphene composite. Inset shows the corresponding pore-size distribution.

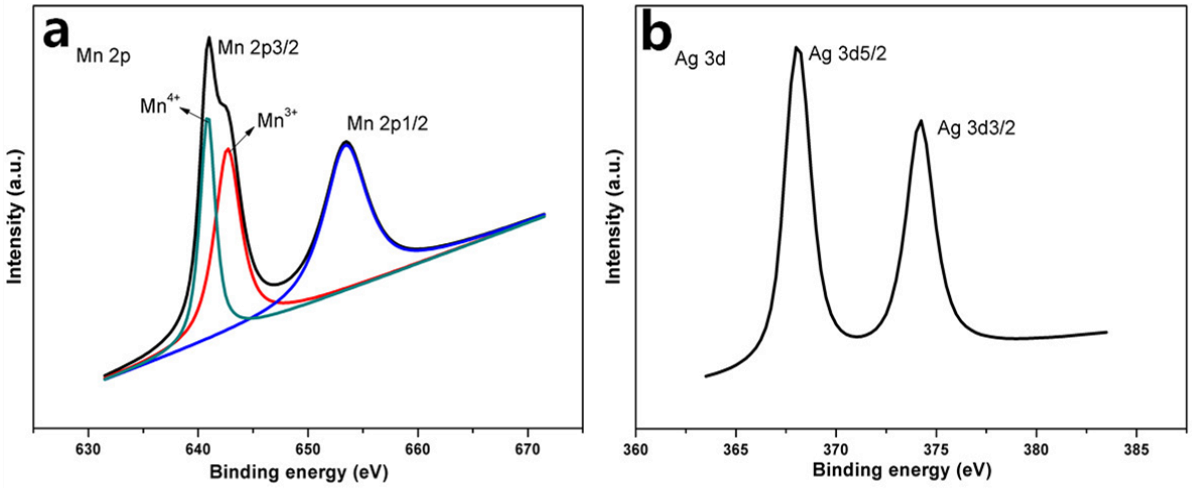

Figure 5. XPS spectra of the Ag-MnO_2/graphene composite: (a) Mn 2p and (b) Ag 3d.

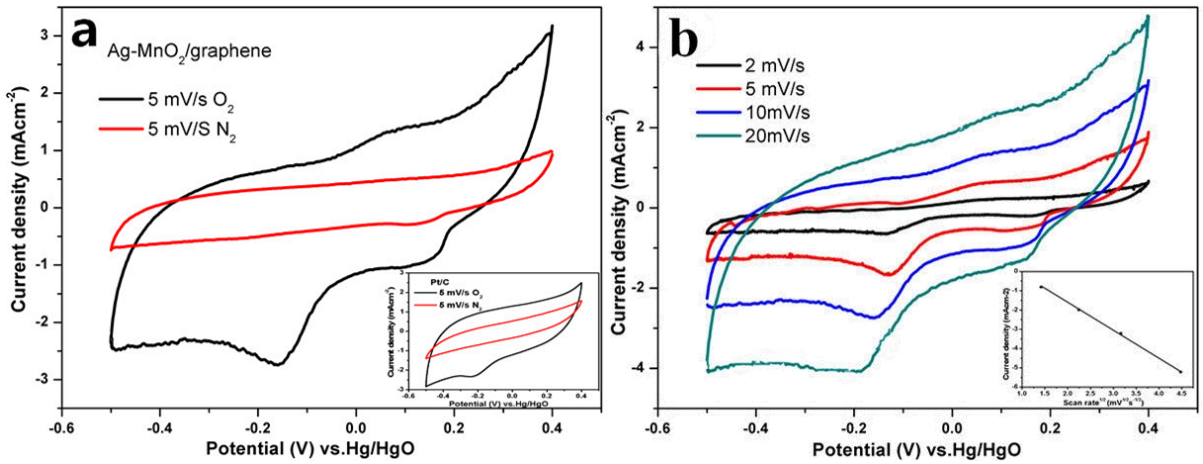

Figure 6. (a) CV of the Ag-MnO_2/graphene and Pt/C (the inset of Figure a) electrode at scan rate of 5 mV/s with the rotation rate at 1200 rpm in a 0.1 M KOH solution saturated with N_2 and O_2, (b) CV of the Ag-MnO_2/graphene electrode at different scan rates with the rotation rate at 1200 rpm in a 0.1 M KOH solution saturated with O_2 and the inset shows the peak current as a function of different rate.

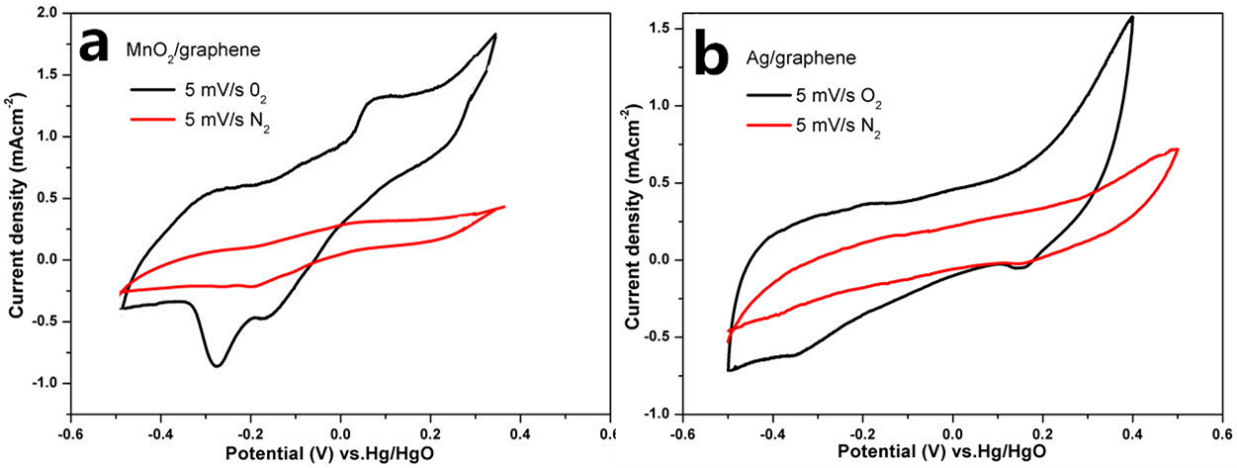

Figure 7. CVs of the different electrode at scan rate of 5 mV/s with the rotation rate at 1200 rpm in a 0.1 M KOH solution saturated with N_2 and O_2: (a) MnO_2/graphene composite, (b) Ag /graphene composite.

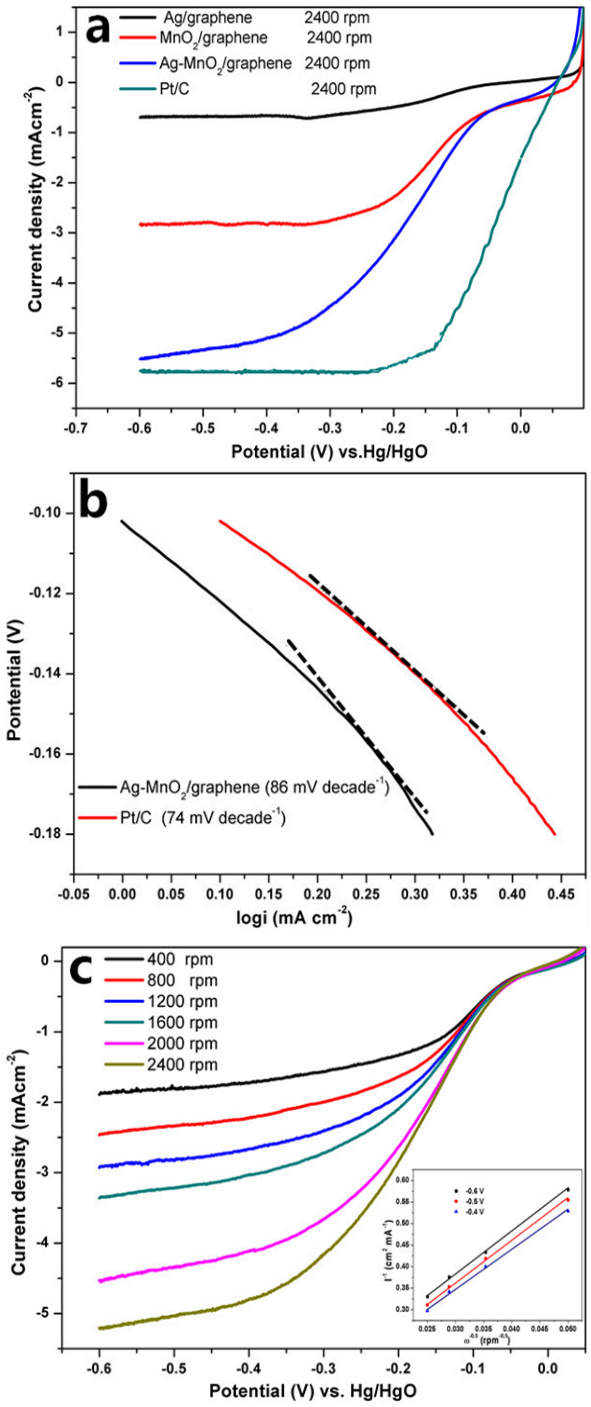

Figure 8. LSV curves (a) of the Ag/graphene, MnO_2/graphene, Ag-MnO_2/graphene and Pt/C catalysts in a 0.1 M KOH solution with O_2-saturated at 2400 rpm with the scanning rate of 1 mV/s, (b) the corresponding Tafel plots. (c) LSV curves of the Ag-MnO_2/graphene composite in a 0.1 M KOH solution with O_2-saturated at different rotation rate with the scanning rate of 1 mV/s and the inset shows the corresponding Koutecky-Levich plots at potentials of −0.4, −0.5, and 0.6 V, respectively.

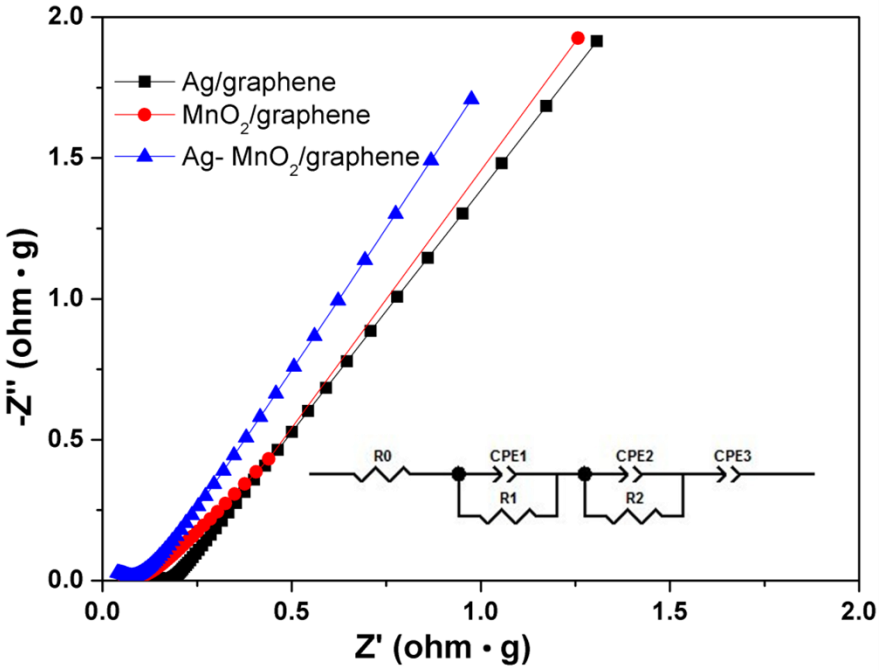

Figure 9. the EIS results of Ag/graphene, MnO_2/graphene and Ag-MnO_2/graphene in 0.1 M KOH solution and the equivalent circuit of the electrodes (inset). 298 K.